

Effect of Water Solubility on Carbon Dioxide Foam Flow in Porous Media: An X-ray Computed Tomography Study

Dong-Xing Du,[†] Ali Naderi Beni,^{‡,§} Rouhollah Farajzadeh,[‡] and Pacelli L. J. Zitha^{*‡}

Qingdao University of Science and Technology, Songling Road 69, 266061, Qingdao, P. R. China, and Delft University of Technology, Stevinweg 1, 2628 CN, Delft, The Netherlands

Carbon dioxide (CO₂) has found wide application in the water-alternating-foam (WAF) processes for enhanced oil recovery (EOR), but few research works have been reported concerning the effect of water solubility on the CO₂ foam rheology in a porous medium. In this paper, an X-ray computed tomography (CT) study is carried out to investigate CO₂ foam flow in a consolidated Bentheimer sandstone core saturated with surfactant solution under different system pressures. As a contrast gas with much lower solubility, nitrogen foam flow is also investigated to show the essence of gas solubility effects. Careful considerations were made on the selection of contrast gases, surfactant, and experimental procedures to focus on the effect of water solubility of the gas on foam rheology in porous media. It is observed from the experiments that CO₂ foam has lower pressure loss and clearly suppressed entrance effect. With the increment of system pressure, the liquid saturation increases and the pressure loss decreases significantly for CO₂ foam flow in the sample core, while little change can be observed for N₂ foam flow. It can be concluded that water solubility is one of the important influential factors for CO₂ foam rheology in porous media.

1. Introduction

When gas and surfactant solution are injected into a porous medium, gas is dispersed into the liquid phase forming foam.¹ A crucial application of foam is in enhanced oil recovery (EOR) projects that aim to produce more oil from underground formations.² For example, water alternating gas (WAG) has been regularly used in the field as a gas-flood mobility control measure. Nevertheless, WAG has not always demonstrated the desired beneficial mobility effects due to the gravity segregation and the unstable preceding of the front between the water and more-mobile gas.^{3,4} Adding surfactant to the aqueous phase has proved to increase the total recovery significantly by creating foam that increases the apparent viscosity of the system.^{5–9}

There are many attractive features of EOR using CO₂ foam injection. First, carbon dioxide is a proven solvent for reconnecting, mobilizing, and recovering waterflood residual oil. Many studies show that it can achieve miscible-like displacement efficiency through multiple contacts (partitioning and extraction) with the crude oil.¹⁰ Second, CO₂ is available naturally in large quantities and as a byproduct of lignite gasification and many manufacturing processes. Its price is also low, and there are no other large volume uses competing for CO₂. Third, with the push toward sustainable power production and the increasing realization for the need to reduce CO₂ emissions, EOR using CO₂ is becoming an important alternative for geological CO₂ storage.

Therefore, lots of laboratory studies concerning the CO₂ foam in EOR have been carried out, including displacement tests, model construction, surfactant screening, etc.^{11–16} Because of the fact that CO₂ is highly soluble in hydrocarbon oils, there are also many research works focusing on the oil solubility effect of CO₂. Holm et al.¹⁷ concluded from experimental study that

CO₂ could enhance the recovery of oil from porous rock by swelling the oil due to its high oil solubility. Monger¹⁸ found the presence of nitrogen had an adverse effect on the CO₂ solubility in oil while sulfur dioxide increases the solubility. Chung et al.¹⁹ measured the solubility of CO₂ in Canyon and Wilmington heavy oils and found that the solubility of CO₂ increased with pressure but decreased with temperature and reduced API gravity. Nguyen et al.²⁰ investigated the effect of nitrogen on the solubility and diffusivity of CO₂ into oil and oil recovery in WAG process and found that the presence of nitrogen could reduce the solubility and diffusivity of carbon dioxide, which results in a reduction in oil recovery.

Albeit the above survey shows the solubility of CO₂ into oil has been extensively investigated, the solubility of CO₂ into water has received little attention so far. As we know, in a water alternating foam (WAF) process, CO₂ exists with not only hydrocarbon oils but also aqueous foams. Gas dissolution in the water phase, like its dissolution in oil phase, is also important as it can modify interfacial tensions, fluid saturations, and hence the foam rheology. Therefore, it is important to examine the effect of solubility of CO₂ into water on the foam rheology in the porous media through experimental studies.

In this paper, two types of gases with large water solubility contrast, CO₂ and N₂, are injected with a surfactant (SDS) solution into a surfactant-saturated sandstone core. Liquid displacement by foam (LDF) along the core is monitored with the aid of X-ray computed tomography (CT), and taking the system pressure as a control parameter, the experiment continues under various backpressures. CT images are investigated to reveal the dynamic foam flow process inside the sandstone core. The comparison of pressure drops, and in situ water saturation profiles between the two kinds of foam flows are presented to give a better understanding of the effect of water solubility on foam rheology.

However, there easily arises a question, and that is how the selection of the contrast gases and the surfactant solution with the experimental procedure can clarify separately the water solubility effect of CO₂ gas. Foam is a complex system, and its behavior in porous media depends on various factors, especially

* To whom correspondence should be addressed. E-mail: p.l.j.zitha@tudelft.nl. Phone: +31 15 278 8437.

[†] Qingdao University of Science and Technology.

[‡] Delft University of Technology.

[§] Now at Applied Geophysics and Geothermal Energy, E.ON Energy Research Center, RWTH Aachen University, Germany.

on the composition of external phase (surfactant type, surfactant concentration, extra additives, salinity, pH, oil presence, etc.), foam quality, and internal gas phase properties.

The criteria for a good CO₂ foamer agent are mainly focused on the generated foam washout stability, adsorption on the rock, foam stability to flowing, residual oil and pH values of aqueous phase.^{21–23} The surfactants ever reported for CO₂ foam studies are Alipal CD-128 (an ammonium salt of linear alcohol ethoxylate sulfate),²⁴ α -olefin sulfonate (AOS),^{25,26} Chaser CD 1040 (alkyl sulfonate),²⁷ Neodol 25-9 (a C12-15 nonionic alcohol ethoxylate),²⁸ Chaser CD 1045 (a proprietary mixture of anionic and nonionic surfactants),^{24,29} and the popular commercial pure chemical of sodium dodecyl sulfate (SDS).^{30,31} Because of the commercial considerations, there are even no names for the surfactants in some published articles.^{32,33} It can be summarized, though, that the most popular surfactants for generating CO₂ foam are anionic or nonionic ones with sulfate or sulfonate bases. Both the pressure drop across a small sandpack, and the interfacial tension between the air and surfactant solution become stable once the critical micelle concentration (cmc) is exceeded.²⁶ So it is usually safe to use the solution with surfactant concentration well above the cmc. Another parameter in external phase which maybe leads to the different foam behavior for CO₂ and N₂ gas is the pH values of the solution. Relatively new capabilities to measure pH in the presence of CO₂ under high pressure (up to 1500 psig) and high temperature (up to 280 °F) indicate pH values in the range of 3.5–4.1 for CO₂ foam under down hole conditions.³⁴ Fortunately, some pioneer researchers have revealed clearly that lower pH values have little effect on foam viscosity,³⁴ foam resistivity,³⁵ or foam stability when the surfactant concentration are higher than the cmc.²²

In our studies, the commercial anionic surfactant SDS was used, and its concentration in external phase was well above the cmc. In all of the experiments the salt concentration remained unchanged, and no oil was present. Therefore, we can conclude the surfactant solution employed in the experiments could not introduce side effects to our contrast gas foam systems. In other words, the different behaviors observed for CO₂ and N₂ foams could not come from the external phase in our experiments. Actually, to compare CO₂ and N₂ foam flow behaviors, quite a few researchers employed same surfactant solution for drawing reasonable conclusions.^{24,27,36}

The foam behavior in porous media also heavily rely on foam quality.^{27,28,37,38} As it is pointed out,²⁷ foam exhibits at least two steady-state flow regimes as a function of foam quality f_g (injected gas volume fraction, %). At high foam qualities, pressure gradient is nearly independent of gas flow rate. This “high-quality” or “coalescence” regime is controlled by bubble coalescence at the “limiting capillary pressure” P_c^* (Pa). In the “low-quality regime”, pressure gradient is nearly independent of liquid flow rate. The transition between regimes occurs at a critical foam quality f_g^* . These two foam-flow regimes are reported with both N₂ and CO₂ gas, with various surfactants, and in various porous media. It is true that CO₂ foam and N₂ foam could be in different foam regimes at the same foam quality, but lying in different foam regimes does not mean necessarily the pressure gradient for each foam system should have much difference. Therefore, we cannot explain from the two-regime theory why f_g^* and pressure gradients for CO₂ and N₂ foam have different behaviors in porous media and why there is a third regime observed for dense CO₂ foam systems.²⁸ As to our understanding, the two-regime foam theory can successfully reveal the foam generation mechanism in porous media,

but it cannot answer the question why different gas foam systems exhibit different pressure gradients in the same porous media. So we still need to refer to the physical properties of N₂ and CO₂ gases for digging out the reasonable explanations. For example, in ref 27, the researchers compared the CO₂ foam and N₂ foam under same foam qualities, although they were aware of the two-regime theory.

On the basis of the above explanations, we could mainly refer to the different physical properties between CO₂ and N₂ gas (internal phase) for explaining their different foam behaviors. In this paper, the experiments are carried out a constant temperature of $T = 20$ °C and different backpressures below 20 bar, so the compressibility difference can be reasonably neglected due to the fact that CO₂ and N₂ both can be treated as ideal gases. Then the main different physical property between CO₂ and N₂ gas is their water solubility. Therefore, we believe our choice of contrast gases, surfactant solution, and the experimental procedures can focus on the study of CO₂ water solubility effect on foam behaviors in the porous media.

2. Experimental Principles, Apparatus, and Procedures

2.1. Experimental Principles. 2.1.1. Gas Solubility. According to Henry’s law,³⁹ when gas is in equilibrium with a liquid, its partial pressure P (Pa) is directly proportional to solute gas concentration C (mol L⁻¹)

$$P = KC \quad (1)$$

where K is a constant, dependent on the nature of the gas and the solvent and on temperature. The values of K for CO₂ and N₂ in pure water at 25 °C are 2.937×10^6 and 155×10^6 (Pa L mol⁻¹), respectively. The solubility of CO₂ is thus about 50 times higher than N₂, which is a sufficient solubility contrast for our purposes of study.

2.1.2. CT Imaging and Liquid Saturations Calculation. X-ray computed tomography (CT) is a technique which enables the visualization of static structures and dynamic processes within opaque objects by reconstructing the X-ray attenuation coefficients from multidirectional X-ray transmission data. The variation in X-ray attenuation is closely related to density differences within the object. Because density transitions usually correspond to boundaries between materials or phases, these data are often straightforward to interpret. Another important advantage of the CT is its digital output, which leads to the easily quantitative analysis.

The linear attenuation coefficient μ (cm⁻¹) can be defined as^{40,41}

$$\mu = \rho \left\{ \sigma(E) + b \frac{Z_e}{E^{3.2}} \right\} \quad (2)$$

where ρ is the electron density (bulk density) in electrons/cm³, $\sigma(E)$ is the Klein–Nishina coefficient, b is a constant ($= 9.8 \times 10^{24}$), Z_e is the effective atomic number of the chemical species, and E is the X-ray photon energy in keV. The values that come out from the computer attached to the CT scanner are measured in Hounsfield units (HU). The relationship between attenuation coefficient and HU is

$$HU_m = 1000 \times \left(\frac{\mu_m}{\mu_w} - 1 \right) \quad (3)$$

where μ_w displays the water attenuation coefficient: we obtain $HU_m = 0$ for water and $HU_m = -1000$ for air. The following equation is used to compute the liquid saturation S_w from the

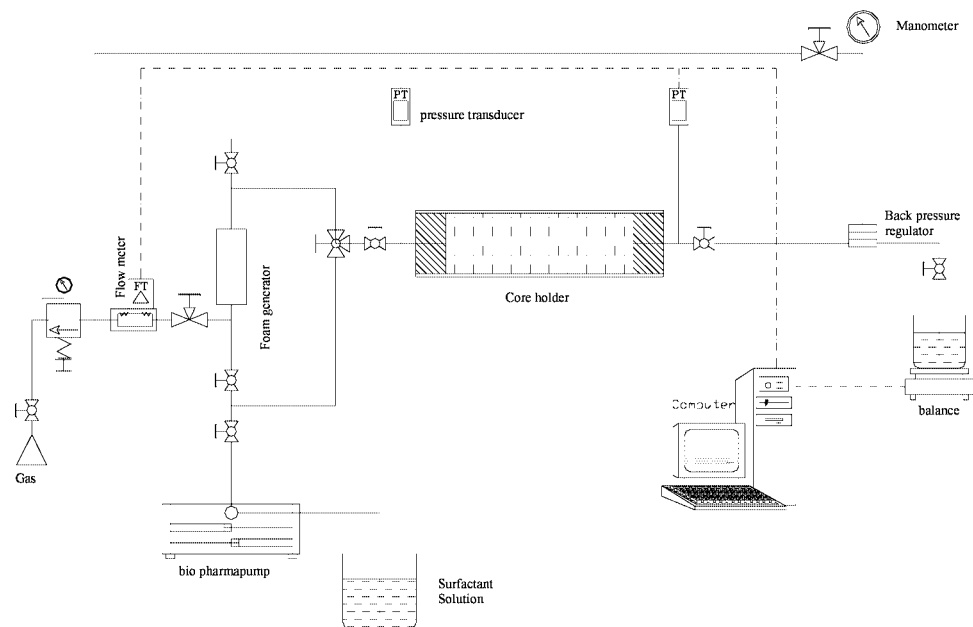


Figure 1. Schematic of the foam flow setup.

measured HU, eliminating the contribution of the rock by the subtraction:⁴²

$$S_w = \frac{HU_{\text{foam}} - HU_{\text{dry}}}{HU_{\text{wet}} - HU_{\text{dry}}} \quad (4)$$

where the subscripts foam, wet, and dry stand for the foam flow, solution saturated, and dry core conditions, respectively. Though theoretically the above equation is only valid under the insoluble conditions, it can still give good estimation for solutions with dissolved CO₂ gas under our experimental conditions due to the fact that there is only negligible density variation coming from the gas dissolution.

2.2. Materials Properties and Preparation. In this work, the surfactant solution is made of sodium dodecyl sulfate (SDS, $M_w = 288$ g/mol) with a concentration of 3.02×10^{-3} M and brine solution of 0.25 M NaCl. The concentration of SDS is above its cmc in 0.25 M NaCl solution, which is reported to be 0.8×10^{-3} M.³¹ To increase the capability of detection, KI (potassium iodide, $M_w = 166$ g/mol) with a concentration of 7.23×10^{-3} M is also added to the surfactant solution. The porous media used to perform the experiments is consolidated Bentheimer sandstone: it is a quartz-rich sandstone, homogeneous and isotropic. The sample core is 180 mm in length and 44 mm in diameter, with the permeability of 1200 mD and the porosity of 22%.

The sample core is drilled out of a massive Bentheimer sandstone block and dehydrated in oven at 60 °C for at least 2 days. Then it is encapsulated in a 2 mm thin layer of low X-ray attenuation Araldite (CW 2215) glue with the CIBA HY 5160 as hardener. The glue is necessary to prevent possible wall effects; otherwise, fluids would bypass the core and displace along the low resistive interface of core holder and core. Finally, the core is fitted inside a specially designed core holder using O-rings. The core holder is fabricated of poly(ether ether ketone) (PEEK) and has good mechanical properties and also low X-ray attenuation. The inner diameter of the PEEK tube is 48.0 mm, and the total length is 220.0 mm.

2.3. Foam Flow Setup and CT-Imaging Settings. The experimental setup used to perform the experiments is shown schematically in Figure 1. It consists of four parts: foam

Table 1. Settings of the CT Scan Measurement

parameter	value
tube current (mA)	100
tube voltage (kV)	125
slice thickness (mm)	1
number of slices	47
effective slices	45
scan mode	spiral
pixels in one CT image	512 × 512

generation part, testing part, pressure controlling part, and data acquisition part.

In the foam generation part, located before the inlet of core holder, gas is mixed with the surfactant solution to make foam. In order to ensure the supply of gas at stable rate, gas flow rate is controlled by using a high-precision needle valve and is monitored by using a gas flow meter. A high-precision double-effect piston displacement pump (Pharmacia P 500) is used to inject the surfactant solution at a constant rate.

In the testing part, the sample core is placed inside a cylindrical core holder. The foam is introduced from the injection tube, and the liquid production is collected in a glass cup on an electronic mass balance. Two high-precision pressure transducers locate at the inlet and the outlet to monitor the pressure drop along the tube.

The pressure control part connects to the outlet of the core. By using a backpressure regulator and a manometer, we can get different pressures in the system. The data acquisition unit records the gas injection rate, pressure, and liquid production data automatically. All experiments are conducted under isothermal conditions. A local air conditioner provided a constant temperature of 20 °C.

Most of this core-flood setup is positioned on the table of the CT scanner. The PEEK core holder is horizontally placed, parallel to the length of the table. The third-generation SAMA-TOM Volume Zoom Quad slice scanner is used in our work. The main technical information about this machine was provided elsewhere,³¹ and the imaging settings in our experiments are listed in Table 1.

The X-ray tube of the CT scanner is operated at the voltage of 125 kV and the current of 100 mA. The thickness of CT

slice is 1 mm, and one series of scan includes 47 slices. Because of the fact that it is hard to get reliable data at the immediate inlet and outlet cross section, the images and the consequent water saturation analysis are actually carried out based on the 45 slices without taking into account the first and the last slice images. The spiral scan mode is applied for imaging the dynamic foam flow, instead of the more classical sequential scanning. The spiral scan allows fast and continuous acquisition of the data from a complete volume and generates axial images using standard reconstruction kernel after the data interpolation. One typical slice image consists of 512×512 pixels. All HU values in the pixels are added together and divided by the total amount of pixels to get the average HU value for one slice image. Because of the fact that the noise for CT images typically ranges from 3 to 20 HU, it can be estimated that the measurement error is about 2% for the HU values in our experiments.

2.4. Experimental Procedures. The whole experimental procedure are constituted by the following three steps:

a. Core Saturation. To ensure complete core saturation, first air is removed by flushing CO₂ through the core. A CT scan of the dry core is then taken. Next, the core is flushed with brine, and the brine injection is continued for 10 pore volumes at a high backpressure (18 bar) to ensure complete dissolution and removal of CO₂. Then, 17 pore volumes of surfactant solution are injected to satisfy the surfactant adsorption capacity, and finally a solution saturated core CT scan is taken. As for N₂ foam experiments, the processes are similar to those of the CO₂ foam to make the proper comparisons.

b. Foam Injection. To induce foam generation, the surfactant solution and gas are injected simultaneously into the foam generator located before the inlet of the core. Gas flow rate is maintained around 7 mL min⁻¹, and liquid flow rate is fixed at 0.7 mL min⁻¹. It has to be pointed out that the gas flow rate is defined at temperature of 0 °C and absolute pressure of 1 atm (101.325 kPa), while the liquid flow rate is defined at the tube inlet conditions. At first, the backpressure is set to atmospheric. CT scan images are taken during foam flow according to the following sequence:

- One scan every 5 min for first 15 min.
- One scan every 15 min for the following 45 min.
- One scan every half an hour after an hour.

c. System Pressure Alternation. After the measurements under atmospheric backpressure, the experiments continue by increasing the backpressures to gauge pressure of 7.5, 12.5, and 16 bar. CT scan is carried out after the system reaching the steady state. In our experiments, the steady state is notified by the stable pressure drop along the core, continuous liquid production, and the stable average gas injection rate.

3. Results and Discussion

To scrutinize the effect of water solubility of CO₂ on the foam rheology in a porous medium, the foam of nitrogen, a gas with much lower water solubility, is also studied to make essential comparisons. At first, comparisons are made for the liquid displacement by foam (LDF) process under the atmospheric backpressure, and then taking the system pressure as a control parameter, comparisons between the two kinds of gas foams continue under higher backpressures.

3.1. Comparison of CO₂ and N₂ Foam at Atmospheric Backpressure. As a base case, the CO₂ and N₂ foam propagation in porous media are studied respectively at atmospheric backpressure. The comparison of the measured parameters, including gas injection rate, pressure drop, and liquid productions, between the CO₂ and N₂ foam flow are presented to give

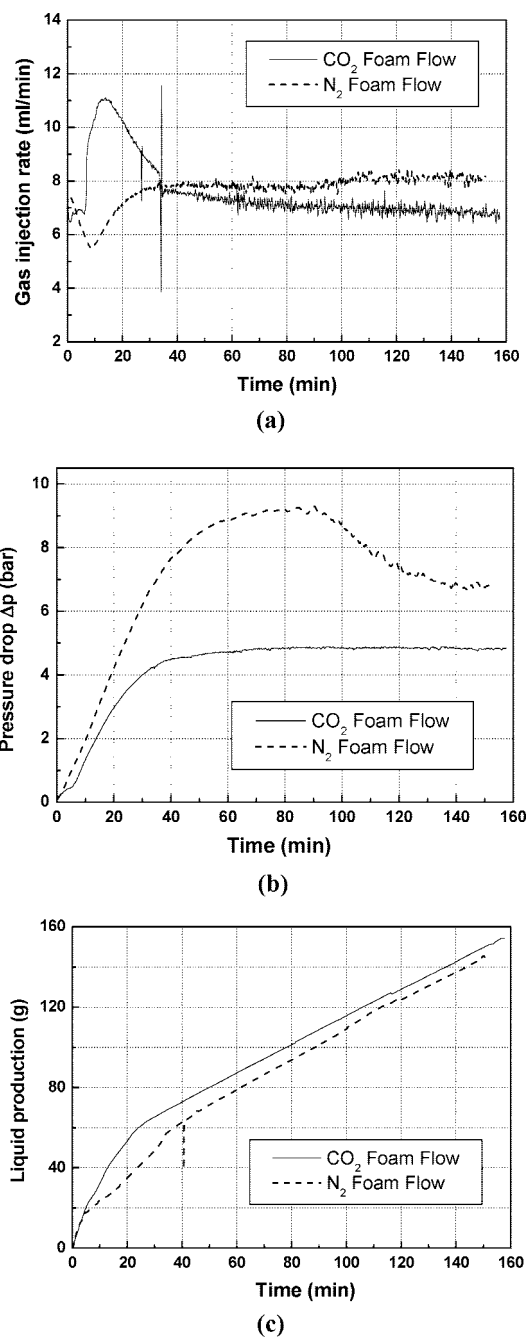


Figure 2. Comparisons of different parameters for CO₂ and N₂ foam flows: (a) gas injection rate, (b) pressure drop, and (c) liquid production.

a clear picture of the differences for two kinds of gas foams. Then more detailed investigations are carried out based on the CT images and water saturation profiles.

3.1.1. Profiles for Gas Injection Rate, Pressure Drop, and Liquid Production. Comparisons between CO₂ and N₂ foam flow in porous media are presented in Figure 2, based on the measured parameters of gas injection rate, pressure drop, and the liquid production.

From Figure 2a we can see the remarkable difference between CO₂ and N₂ injection rates in the first 35 min. The injection rate for CO₂ is obviously higher than N₂. After 35 min, the gas injection rates for both gases are maintained at about 7 mL min⁻¹.

From Figure 2b, it can be seen that in the first 5 min the pressure drop for CO₂ and N₂ foam is nearly the same, but after that, the pressure drop for N₂ foam flow increases more rapidly

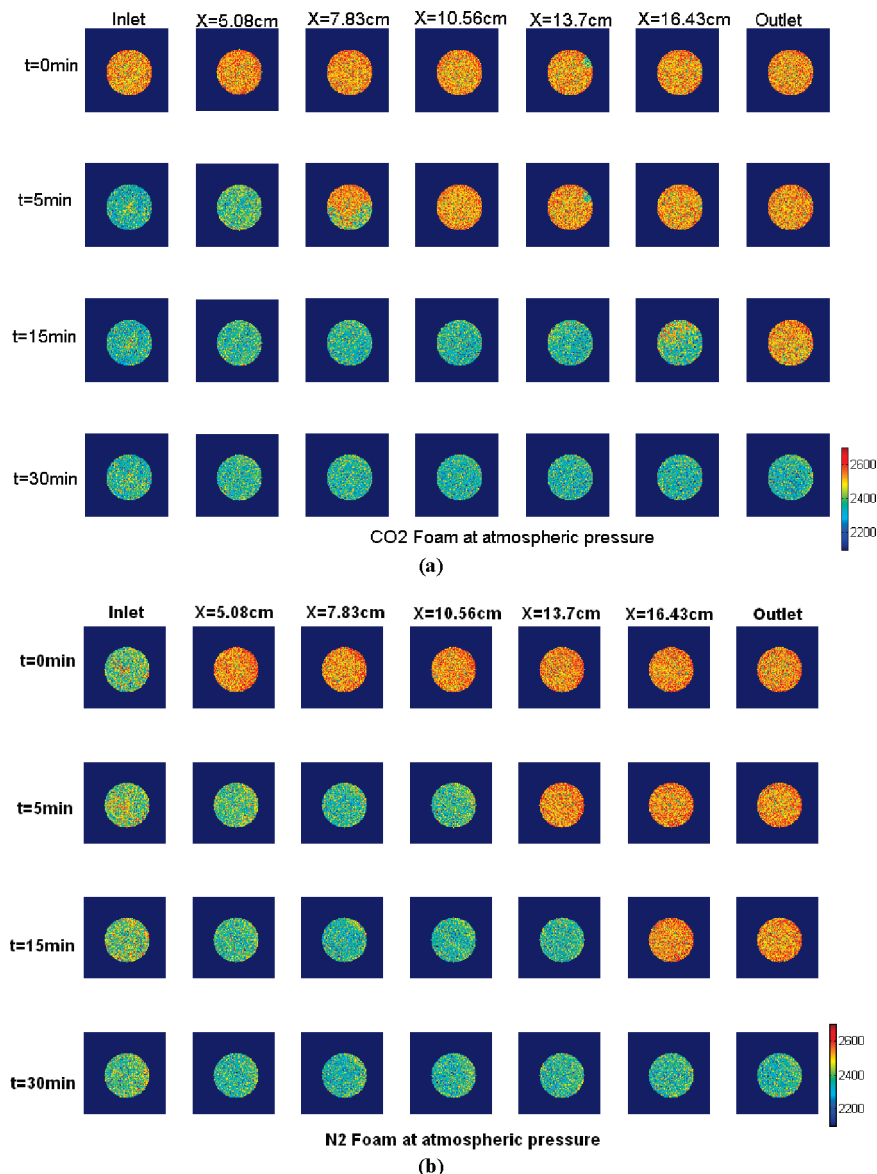


Figure 3. CT images for foam development in the sample core at atmospheric backpressure: (a) CO₂ foam; (b) N₂ foam.

than that of CO₂ foam. The higher pressure drop for N₂ foam is quite meaningful, given that the flow rate for N₂ foam is lower than CO₂ foam in the time span of 5–35 min after injection. The pressure drop profile for CO₂ foam becomes flat after 60 min, with a value around 5 bar, while the N₂ foam has a peak pressure drop at 90 min after the injection and finally gains a stable value of 7 bar after 140 min.

The liquid productions for two kinds of foams are presented in Figure 2c. Because of the gas rate difference in the beginning of the foam injection, it can be observed that liquid production for CO₂ foam is higher than N₂ foam. However, in general production for CO₂ foam is lower than N₂ foam. This is confirmed by comparing saturation profiles in Figure 4.

The above figures clearly reveal that N₂ foam flow has higher pressure loss than CO₂ foam in porous media. After 5 min of foam injection, the pressure drops for N₂ foam become increasingly higher than CO₂ foam even at the low gas injection rates. When foam injection approaches the steady state, which is reflected by the flat pressure drop and steady gas injection rates, the pressure drop of N₂ foam is also about 2 bar higher than CO₂ foam. Our experimental results are in good agreement with those reported by Gauglitz et al.,^{16,27} who also observed

lower CO₂ foam pressure gradient compared to N₂ foam, even though they employed the Boise sandstone and the surfactant of Chase CD1040.

The lower pressure drop for CO₂ foam is most likely due to its weaker foam strength caused by its high solubility in water. Indeed, some researchers have expressed obscurely their considerations concerning the CO₂ water solubility effect. Valko et al.⁴³ attributed much of the rheology model error to the uncertainty of the CO₂ solubility, while they can describe pure nitrogen experiments with improved accuracy. Bhide et al.²¹ reported that the foam dissolution into the flowing water is the factor limiting the foam lifetime of polymeric surfactant. They declared that at field conditions foam lifetime will depend on dissolved gas content in produced water and type of gas in foam. The possible explanations could refer to Wellington and Vinegar,¹¹ who concluded the dissolved CO₂ can decrease the solubility of surfactant in the aqueous phase, causing lower interfacial tension and thus decrease the apparent foam viscosity.

3.1.2. CT Images Analysis. To investigate the dynamic foam flow process in the sample core in more detail, the CT images of the fluid distribution in slices at various positions along the core (x direction) are examined. Parts a and b of Figure 3 present

respectively a partial set of CT images of the fluid distribution during liquid displacement by CO₂ and N₂ foams in the first 30 min of the gas injection. As mentioned in section 2.3, the inlet and the outlet slices in the figures are actually the slices next to the immediate inlet and outlet cross section, namely, the slices at the position of $X = 0.39$ cm and $X = 17.61$ cm, respectively. To eliminate negative values, the HU numbers calculated by eq 3 are added to a constant of 1000 in the figure demonstration. The orange color, indicating the high HU numbers, corresponds to a core fully saturated with surfactant solution, while the blue color parts in the slices stand for the lower liquid saturation. The first row in Figure 3a shows a core fully saturated with surfactant solution, except for a tiny portion of gas at 13.7 cm. The next rows of images present visually the evolution of liquid saturation accompanying CO₂ foam propagation in the sandcore, with all slices become progressively blue. At 5 min and at position of $X = 7.83$ cm, foam propagation can be observed in the lower part of the core. At the time $t = 30$ min, the last row of images indicates the foam has made a breakthrough in the porous media. Figure 3b presents the nitrogen foam flushing process. Similarly, it can be concluded from the CT images that foam breakthrough occurs between 15 and 30 min.

3.1.3. Saturation Profiles. To analyze quantitatively the evolution of liquid saturation over the core, the CT data is converted into saturation profiles by using eq 4. The saturation distribution in the sample core at different times for CO₂ and N₂ foams flow are shown in parts a and b of Figure 4, respectively.

Both figures show two stages of the liquid displacement by foam. In the first stage, starting from the beginning of the injection up to the foam breakthrough, the so-called piston-like displacement occurs. As can be seen from the figures, the first stage consists of three regions: (a) a region with low liquid saturation, (b) a region with high liquid saturation, and (c) a transition region. For both cases, the low liquid saturation region gradually increases with the elapsing time. The second stage starts after foam breakthrough and ends with the unchanged water saturation distribution. This stage is characterized by secondary liquid desaturation,^{44,45} which starts in the central part of the core and propagates toward the inlet and the outlet. The so-called capillary end effect is eliminated by this secondary desaturation, and consequently the liquid saturation near the outlet is low. However, secondary liquid desaturation does not completely eliminate the entrance effect at the inlet, and consequently the liquid saturation near the core inlet remains relatively high.

Detailed investigation of the two figures reveals remarkable differences between CO₂ and N₂ foams in the foam propagation process in the porous media. First, the penetrating front for N₂ foam is much sharper than CO₂ foam, which can be clearly read by comparing the two sets of data before foam breakthrough. Besides, the displacement front for nitrogen foam becomes steeper with elapsing time, while no such phenomenon can be observed for CO₂ foam. Second, it can be found that, except at the narrow inlet and outlet region, the liquid remaining in the porous media after CO₂ foam sweep is obviously higher than that after N₂ foam penetration, namely, 30% vs 15%. Third, the entrance effect for CO₂ foam displacement is much less significant than N₂ foam. As shown in Figure 4a, the entrance length for CO₂ foam is about 4 cm, while it is about 6 cm for N₂ foam shown in Figure 4b. After 60 min of gas injection, the entrance effect can be reasonably neglected for CO₂ foam, but the entrance effect for N₂ foam flow exists even after 150 min of gas injection. Because of the large contrast on the water

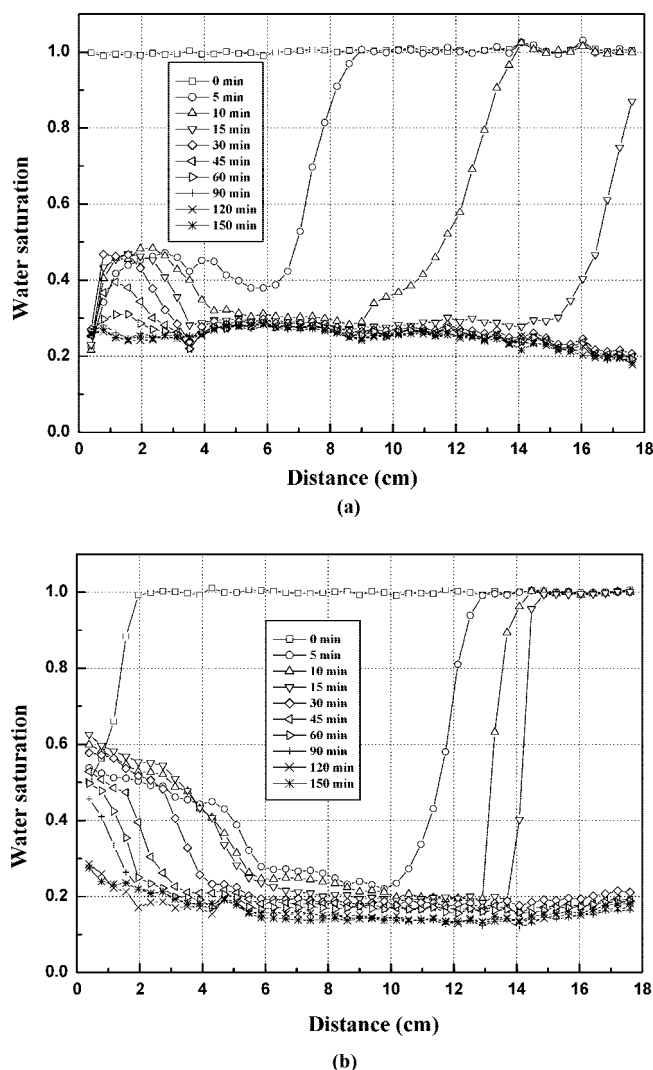


Figure 4. Water saturation profile in different times at atmospheric pressure: (a) CO₂ foam; (b) N₂ foam.

Table 2. Comparison for CO₂ and N₂ Foam Flow under Different Backpressures

backpressure (gauge pressure) P_b (bar)	CO ₂ foam flow		N ₂ foam flow	
	pressure drop Δp (bar)	gas injection rate Q (mL min ⁻¹)	pressure drop Δp (bar)	gas injection rate Q (mL min ⁻¹)
0.0	4.8	6.8	7.0	8.0
7.5	0.9	7.5	7.0	6.8
12.5	1.5	7.5	6.0	5.8
16.0	1.5	7.5	7.0	7.5

solubility for CO₂ and N₂, it can be concluded that higher water solubility of the CO₂ is an important factor which results in different foam behaviors.

3.2. Comparison of CO₂ and N₂ Foam at Higher Backpressures. Because of the significant effect of pressure on the gas water solubility, as stressed by Henry's law, system pressure is the main parameter varied in the experiments. As already mentioned, the system pressure is controlled by using a backpressure regulator. The backpressures employed in the experiments are 7.5, 12.5, and 16 bar, respectively.

3.2.1. Pressure Drops and Gas Injection Rates. Table 2 lists the comparisons of pressure drop and average gas injection rate for CO₂ and N₂ foams under different backpressures. It can be seen clearly that the pressure loss for CO₂ foam decreases drastically when the system backpressure increases to 7.5 bar.

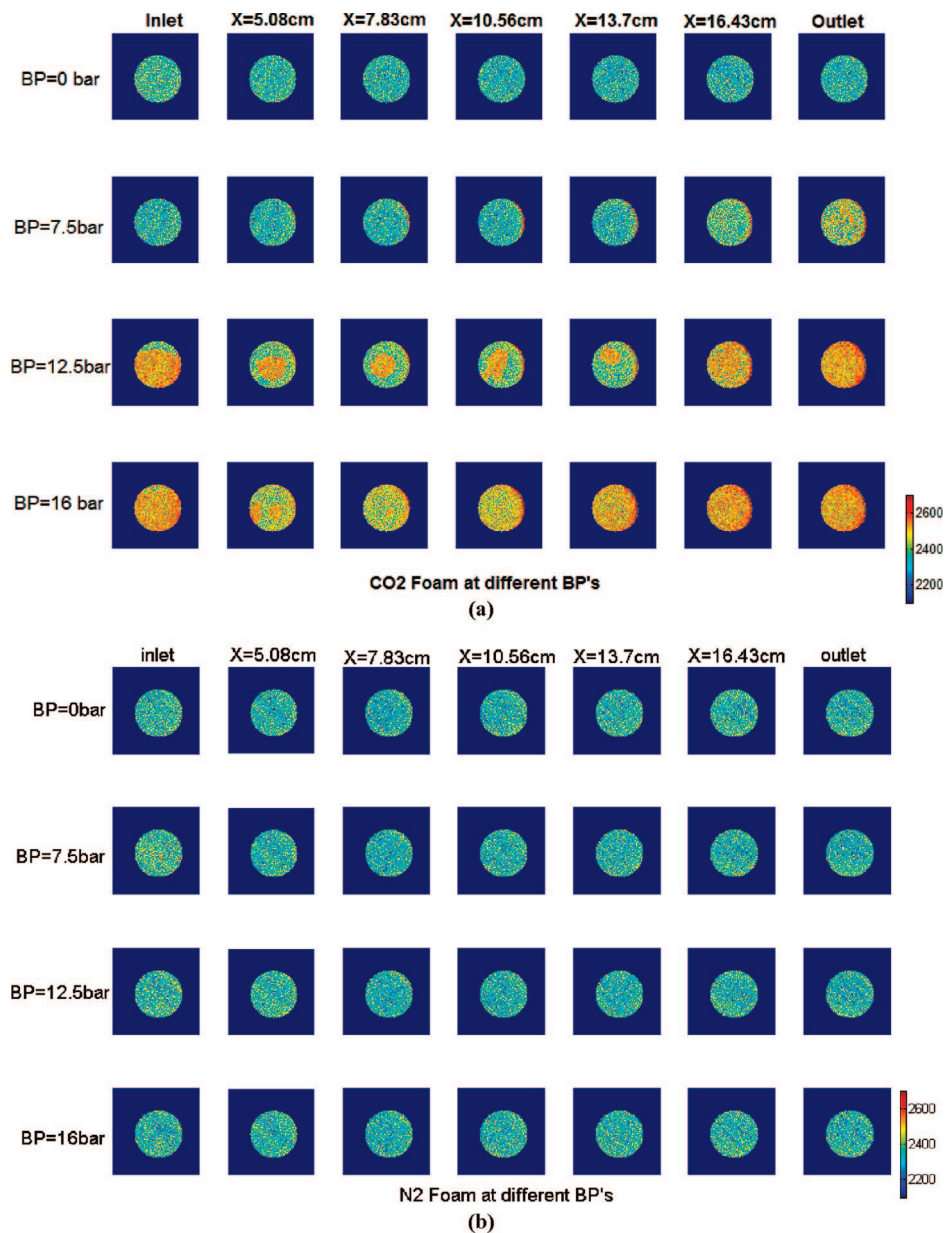


Figure 5. CT images for foam development at different backpressures: (a) CO₂ foam; (b) N₂ foam.

However, the pressure drop does not change much with further system pressure increment. As for the N₂ foam flow, it can be read from the table that the system pressure has little effect to the pressure losses along the sand core, and the pressure drop maintained at about 7.0 bar under all backpressure conditions.

The explanation for the different behavior of two kinds of gases under higher backpressures also lies on the water solubility. With the increment of system pressure the interfacial tension for CO₂ foam decreases with increased water solubility, while the flow characteristics for N₂ foam do not change much for its water insoluble property.

3.2.2. CT Images Analysis. Parts a and b of Figure 5 show CT images of the fluid distribution at different backpressures for CO₂ and N₂ foams, respectively. It is worthy mentioning that for higher pressure experiments the initial state of the sand core is no longer fully solution saturated but is foam saturated at the former system pressure.

Figure 5a reveals that the liquid saturation for CO₂ foam increases as pressure increases. That is because more carbon dioxide molecules dissolve into the water as the pressure increases, referring to the Henry's law. It is also read from the

figure that the dissolution occurs at first in the outlet region, as shown in the second row of images with backpressure of 7.5 bar. Then more carbon dioxide gas is dissolved in the inlet region, as shown in the third row of the figure. Finally, the gas dissolves in the whole sandcore, as indicated in the last row of images under the system backpressure of 16 bar. However, the pressure effect for the N₂ foam, as shown in Figure 5b, cannot be clearly identified due to the low solubility of the nitrogen in the water.

Another obvious phenomenon for CO₂ foam flow, as shown in Figure 5a, is that the liquid phase is no longer uniformly distributed in the cross section of the sandcore under high pressures. For example, at backpressure of 12.5 bar, gas phase concentrates in the upper and lower part while the liquid flows in the center region of the core. However, no such phenomenon happens on nitrogen foam flow, as shown in Figure 5b.

3.2.3. Saturation Profiles. Parts a and b of Figure 6 depict the liquid saturation distribution along the sample for CO₂ foam and N₂ foam flow at different backpressures, respectively.

In accordance with the CT images shown in Figure 5a, Figure 6a shows quantitatively the trend that higher pressure leads to

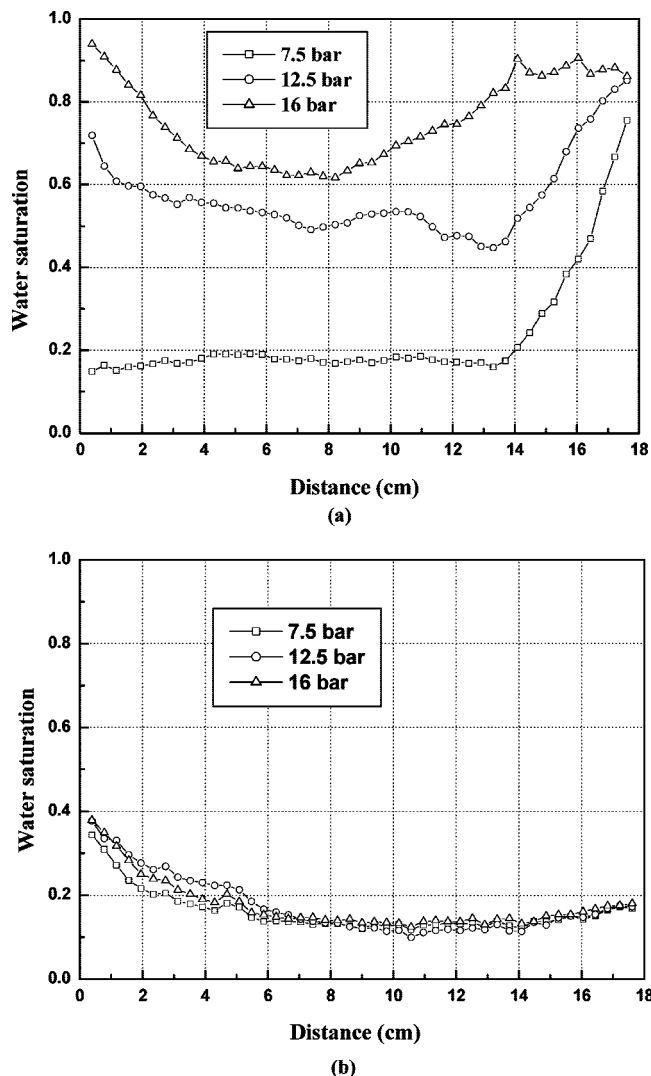


Figure 6. Water saturation profile at different backpressures: (a) CO₂ foam; (b) N₂ foam.

higher liquid saturation for CO₂ foam. When the backpressure increases to 7.5 bar, the dissolution of carbon dioxide appears first in the outlet part, more exactly, the region of $X = 14\text{--}18$ cm on the length direction of the sandcore, with the maximum liquid saturation value of 0.8 at the outlet. This is because the increment of the backpressure causes a quick dissolution of the CO₂ gas at the outlet, thus showing a temporary “shut-in” of the effluence at that region. When the backpressure increases to 12.5 bar, the higher system pressure leads to higher CO₂ dissolution at the inlet region, namely 0–4 cm region of the sample, where the liquid saturation values grow faster compared to the center and the outlet part. With the further increment of system pressure, the water saturation increases unanimously in nearly the whole sample, with the exception of the region very near to the outlet. Under the backpressure of 16 bar, the water saturation nearly equals unity at the inlet, indicating no foam phase at the entrance of the core.

It can be concluded from Figure 6b that the effect of the pressure on the liquid saturation can be reasonably neglected for N₂ foam, which agrees well with the above pressure drop results in Table 2 and the CT scan images shown in Figure 5b.

4. Conclusion

A computer tomography (CT) study is carried out to study the CO₂ and N₂ foam flow in a consolidated Bentheimer

sandstone core sample initially saturated with surfactant solution. Comparisons between the two kinds of foam flow are made to investigate the effect of water solubility on the foam propagation process in a porous medium by taking the system pressure as control parameter. The conclusions are listed as follows:

(1) Pressure drop measurements show lower pressure loss for CO₂ foam than N₂ foam flow in porous media. An important factor leading to this difference lies on the higher water solubility of the CO₂ gas. It is believed that the dissolved CO₂ can decrease the solubility of surfactant in the aqueous phase, causing lower interfacial tension and thus decrease the apparent foam viscosity.

(2) CT images analysis and the consequent liquid saturation results reveal that the propagation front for CO₂ foam is not the exact piston-like, as shown in the N₂ foam injection process. The remaining liquid content in the sandcore is also higher after CO₂ foam sweep. The experimental observations are in good agreement with the pressure drop measurements, indicating the lower CO₂ foam apparent viscosity.

(3) The quantitative liquid saturation profiles reveal that the entrance effect for CO₂ foam propagation is much less significant than it is for N₂ foam. Part of this difference can be explained by the higher water solubility of CO₂ gas.

(4) Pressure measurements, CT images, and water saturation profiles analysis show that the increment of system pressure can decrease the pressure drop and increase the liquid saturation significantly for CO₂ foam flow in porous media, while it has little effect on the N₂ foam flow.

Acknowledgment

We thank Peter de Vreede and Adri Maljaars for technical support. The experiments were conducted using the X-ray computer tomography apparatus funded by the Dutch Technology Foundation (STW) through Project DAR.5756.

Literature Cited

- (1) Exerowa, D.; Kruglyakov, P. M. *Foam and Foam Films: Theory, Experiments, Application*; Elsevier: New York, 1998.
- (2) Rossen, W. R. Foams in enhanced oil recovery. In *Foams: Theory, Measurements and Applications*; Prud'homme, R. K., Khan, S., Eds.; Marcel Dekker: New York, 1996; pp 413–464.
- (3) Holm, L. W. Evolution of the Carbon-Dioxide Flooding Processes. *J. Pet. Technol.* **1987**, *39*, 1337.
- (4) Smith, D. H. Promise and Problems of Miscible-Flood Enhanced Oil Recovery: The Need for Surfactant-Based Sweep and Mobility Control. In *Surfactant Based Mobility Control—Progress in Miscible Flood Enhanced Oil Recovery*; Smith, D. H., Ed.; ACS Symposium Series 373; American Chemical Society: Washington, DC, 1988; pp 2–37.
- (5) Holm, L. W. The Mechanism of Gas and Liquid Flow through Porous Media in the Presence of Foam. *SPE J.* **1968**, *8*, 359.
- (6) Ali, J.; Burley, R. W.; Nutt, C. W. Foam Enhanced Oil-Recovery from Sand Packs. *Chem. Eng. Res. Des.* **1985**, *63*, 101.
- (7) Patzek, T. W. Field Application of Foam for Mobility Improvement and Profile Control. *SPE Reservoir Eng.* **1996**, *11*, 79.
- (8) Zhdanov, S. A.; Amiyani, A. V.; Surguchev, L. M.; Castanier, L. M.; Hanssen, J. E. Application of Foam for Gas and Water Shut-off: Review of Field Experience. SPE 36914 in European Petroleum Conference, Milan, Italy, Oct 22–24, 1996.
- (9) Turta, A. T.; Signal, A. K. Field Foam Applications in Enhanced Oil Recovery Projects: Screening and Design Aspect. SPE 48895 in SPE International Oil and Gas Conference and Exhibition in China, Beijing, China, Nov 2–6, 1998.
- (10) Stalkup, F. I., Jr. *Miscible Displacement*; Monograph No. 8; Society of Petroleum Engineers of AIME: New York, 1983.
- (11) Wellington, S. L.; Vinegar, H. J. Surfactant-Induced Mobility Control for Carbon Dioxide Studied with Computerized Tomography. In *Surfactant Based Mobility Control—Progress in Miscible Flood Enhanced Oil Recovery*; Smith, D. H., Ed.; ACS Symposium Series 373; American Chemical Society: Washington, DC, 1988; pp 344–358.

- (12) Claridge, E. L.; Lescure, B. M.; Wang, M. W. Carbon Dioxide Foam Flooding, Laboratory Model and Computer Simulation of the Process. In *Surfactant Based Mobility Control—Progress in Miscible Flood Enhanced Oil Recovery*; Smith, D. H., Ed.; ACS Symposium Series 373; American Chemical Society: Washington, DC, 1988; pp 359–374.
- (13) Lee, H. O.; Heller, J. P. Carbon Dioxide-Foam Mobility Measurements at High Pressure. In *Surfactant Based Mobility Control—Progress in Miscible Flood Enhanced Oil Recovery*; Smith, D. H., Ed.; ACS Symposium Series 373; American Chemical Society: Washington, DC, 1988; pp 375–386.
- (14) Patton, J. T.; Holbrook, S. T. Enhancement of Crude Oil Recovery in Carbon Dioxide Flooding. In *Surfactant Based Mobility Control—Progress in Miscible Flood Enhanced Oil Recovery*; Smith, D. H., Ed.; ACS Symposium Series 373; American Chemical Society: Washington, DC, 1988; pp 387–404.
- (15) Kuhlman, M. I.; Lau, H. C.; Falls, A. H. Surfactant Criteria for Successful Carbon Dioxide Foam in Sandstone Reservoirs. *SPE Reservoir Eval. Eng.* **2000**, *3*, 35.
- (16) Gauglitz, P. A.; Friedmann, F.; Kam, S. I.; Rossen, W. R. Foam Generation in Homogeneous Porous Media. *Chem. Eng. Sci.* **2002**, *57*, 4037.
- (17) Holm, L. W.; Josendal, V. A. Mechanism of Oil Displacement by Carbon Dioxide. *J. Pet. Technol.* **1974**, *26*, 1427.
- (18) Monger, T. G. Measurement of Immiscible CO₂ Injection in Heavy Oil Reservoirs. *Ind. Eng. Chem. Res.* **1987**, *26*, 1147.
- (19) Chung, F. T. H.; Jones, R. A.; Nguyen, H. T. Measurement and Correlations of the Physical Properties of CO₂/Heavy-Crude-Oil Mixtures. *SPE Reservoir Eng.* **1988**, *3*, 822.
- (20) Ngyuen, T. A.; Farouq, A. S. M. Effect of Nitrogen on the solubility and diffusivity of Carbon Dioxide into Oil and Oil Recovery by the Immiscible WAG Process. *J. Can. Pet. Technol.* **1998**, *37*, 24.
- (21) Bhide, V.; Hirasaki, G.; Miller, C.; Puerto, M. Foams for Controlling Water Production SPE 93273 in SPE International Symposium on Oilfield Chemistry, the Woodlands, TX, Feb 2–4, 2005.
- (22) Liu, Y.; Grigg, R. B. Salinity, pH, and Surfactant Concentration Effects on CO₂-Foam. SPE 93095 in SPE International Symposium on Oilfield Chemistry, the Woodlands, TX, Feb 2–4, 2005.
- (23) Grigg, R. B.; Bai, B. Sorption of Surfactant Used in CO₂ Flooding onto Five Minerals and Three Porous Media. SPE 93100 in SPE International Symposium on Oilfield Chemistry, the Woodlands, TX, Feb 2–4, 2005.
- (24) Holm, L. W.; Garrison, W. H. CO₂ Diversion With Foam in an Immiscible CO₂ Field Project. *SPE Reservoir Eng.* **1988**, *3*, 112.
- (25) Lee, H. O.; Heller, J. P. Laboratory Measurements of CO₂-Foam Mobility. *SPE Reservoir Eng.* **1990**, *5*, 193.
- (26) Bertin, H. J.; Apaydin, O. G.; Castanier, L. M.; Kovscek, A. R. Foam Flow in Heterogeneous Porous Media: Effect of Cross Flow. *SPE J.* **1999**, *4*, 75.
- (27) Gauglitz, P. A.; Friedmann, F.; Kam, S. I.; Rossen, W. R. Foam Generation in Porous Media. SPE 75177 in SPE/DOE Improved Oil Recovery Symposium, Tulsa, OK, April 13–17, 2002.
- (28) Kim, J. S.; Dong, Y.; Rossen, W. R. Steady-State Flow Behavior of CO₂ Foam. *SPE J.* **2005**, *10*, 405.
- (29) Bai, B.; Grigg, R. B. Kinetics and Equilibria of Calcium Lignosulfonate Adsorption and Desorption onto Limestone. SPE 93098 in SPE International Symposium on Oilfield Chemistry, the Woodlands, TX, Feb 2–4, 2005.
- (30) Du, D. X.; Zitha, P. L. J.; Uijtjenhout, M. G. H. Carbon Dioxide Foam Rheology in Porous Media: A CT Scan Study. *SPE J.* **2007**, *12*, 245.
- (31) Nguyen, Q. P. Dynamics of Foam in Porous Media. Ph.D. Thesis, Delft University of Technology, Delft, The Netherlands, 2004.
- (32) Harris, P. C. Rheology of Crosslinked Foams. *SPE Prod. Facil.* **1996**, *11*, 113.
- (33) Harris, P. C. A. Comparison of Mixed Gas Foams With N₂ and CO₂ Foam Fracturing Fluids on a Flow Loop Viscometer. *SPE Prod. Facil.* **1995**, *10*, 197.
- (34) Fredd, C. N.; Miller, M. J.; Quintero, B. W. Impact of Water-Based Polymer Fluid Characteristics on CO₂ Foam Rheology. SPE 86493 in SPE International Symposium and Exhibition on Formation Damage Control, Lafayette, LA, Feb 18–20, 2004.
- (35) Zhu, T.; Strycker, A.; Raible, C. J.; Vineyard, K. Foams for Mobility Control and Improved Sweep Efficiency in Gas Flooding. SPE 39680 in SPE/DOE Improved Oil Recovery Symposium, Tulsa, OK, April 19–22, 1998.
- (36) Hutchins, R. D.; Miller, M. J. A Circulating Foam Loop for Evaluating Foam at Conditions of Use. *SPE Prod. Facil.* **2005**, *20*, 286.
- (37) Cheng L.; Reme A. B.; Shan D.; Coombe D. A.; Rossen W. R. Simulating Foam Processes at High and Low Foam Qualities. SPE 59287 in SPE/DOE Improved Oil Recovery Symposium, Tulsa, OK, April 3–5, 2000.
- (38) Kam, S. I.; Rossen, W. R. A Model for Foam Generation in Homogeneous Media. *SPE J.* **2003**, *8*, 417.
- (39) Henrys-law.Org. <http://www.mpch-mainz.mpg.de/~sander/res/henry.html> (accessed Feb 7, 2008).
- (40) McCullough, E. C. Photon Attenuation in Computed Tomography. *Med. Phys.* **1975**, *2*, 307.
- (41) Vinegar, H. J.; Wellington, S. L. Tomographic Imaging of three-phase Flow Experiments. *Rev. Sci. Instrum.* **1987**, *58*, 96.
- (42) Nguyen, Q. P.; Currie, P. K.; Zitha, P. L. J. Effect of Cross-Flow on Foam-Induced Diversion in Layered Formations. *SPE J.* **2005**, *10*, 54.
- (43) Valko, P.; Economides, M. J.; Baumgartner, S. A.; McElfresh, P. M. The Rheological Properties of Carbon Dioxide and Nitrogen Foams. SPE 23778 in SPE Formation Damage Control Symposium, Lafayette, LA, Feb 26–27, 1992.
- (44) Nguyen, Q. P.; Currie, P. K.; Zitha, P. L. J. Determination of Foam Induced Fluid Partitioning in Porous Media using X-ray Computed Tomography. SPE 80245 in SPE International Symposium on Oilfield Chemistry, Houston, TX, Feb 5–7, 2003.
- (45) Zitha, P. L. J.; Nguyen Q. P.; Currie, P. K. Effect of Flow Velocity and Rock Layering on Foam Flow: an X-ray Computed Tomography Study. SPE 80530 in SPE Asia Pacific Oil and Gas Conference and Exhibition, Jakarta, Indonesia, Sept 9–11, 2003.

Received for review December 11, 2007

Revised manuscript received April 25, 2008

Accepted May 6, 2008

IE701688J